ACS APPLIED MATERIALS & INTERFACES

RESEARCH ARTICLE

www.acsami.org

Synthesis of Gadolinium Nanoscale Metal−Organic Framework with Hydrotropes: Manipulation of Particle Size and Magnetic Resonance Imaging Capability

Wilasinee Hatakeyama,[†] Talia J. Sanchez,[†] Misty D. Rowe,[†] Natalie J. Serkova,[‡] Matthew W. Liberatore,[§] and Stephen G. Boyes*[,†]

[†]Department of Chemistry and Geochemistry, Colorado School of Mines, Golden, Colorado 80401, United States

[‡]Department of Anesthesiology and Radiology, University of Colorado, Anschutz Medical Center, Aurora, Colorado 80045, United States

[§]Department of Chemical Engineering, Colorado School of Mines, Golden, Colorado 80401, United States

Supporting Information

ABSTRACT: Gadolinium metal−organic framework (Gd MOF) nanoparticles are an interesting and novel class of nanomaterials that are being studied as a potential replacement for small molecule positive contrast agents in magnetic resonance imaging (MRI). Despite the tremendous interest in these nanoscale imaging constructs, there are limitations, particularly with respect to controlling the particle size, which need to be overcome before these nanoparticles can be integrated into *in vivo* applications. In an effort to control the size, shape, and size distribution of Gd MOF nanoparticles, hydrotropes were incorporated into the reverse microemulsion synthesis used to produce these nanoparticles. A study of how hydrotropes influenced the mechanism of formation of reverse micelles offered a great deal of information with respect to the physical properties of the Gd MOF nanoparticles formed. Specifically, this study incorporated the hydrotropes, sodium salicylate (NaSal), 5-methyl salicylic acid, and salicylic acid into the reverse microemulsion. Results demonstrated that addition of each of the hydrotropes into the synthesis of Gd MOFs provided a simple route to control the nanoparticle size as a function of hydrotrope concentration. Specifically, Gd MOF nanoparticles synthesized with NaSal showed the best reduction in size distributions in both length and width with percent relative standard deviations being nearly 50% less than nanoparticles produced via the standard route from the literature. Finally, the effect of the size of the Gd MOF nanoparticles with respect to their MRI relaxation properties was evaluated. Initial results indicated a positive correlation between the surface areas of the Gd MOF nanoparticles with the longitudinal relaxivity in MRI. In particular, Gd MOF nanoparticles with an average size of 82 nm with the addition of NaSal, yielded a longitudinal relaxivity value of 83.9 mM^{-1} [Gd^{3+}] sec^{-1}, one of the highest reported values compared to other Gd-based nanoparticles in the literature to date.

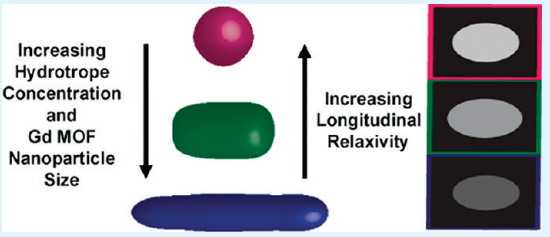

KEYWORDS: gadolinium nanoparticle, hydrotrope, magnetic resonance imaging

INTRODUCTION

Gadolinium (Gd) complexes are widely used in magnetic resonance imaging (MRI) as diagnostic contrast agents because of their strong paramagnetic properties. In the clinical setting, Gd chelates are extensively employed in order to provide positive contrast yielding increased sensitivity; however, their low retention time and difficulty in further functionalization limits their improvement in advanced medical applications such as targeted drug delivery. Furthermore, high dosages of these contrast agents must be given due to the low sensitivity, lack of selectivity, and low retention time, making them effective only in areas of high accumulation. Much effort has been aimed at improving Gd chelate retention times by modifying the chelates themselves with preformed polymers such as albumin,[1] polylysine,[2] dextran,[3−5] dendrimers,[6−11] liposomes,[12−16] and other biocompatible polymers.[5,17,18] Although these results have shown increased retention times and relaxation rates, toxicity and chelate stability continue to be issues.

In an attempt to overcome some of these downfalls, research has recently focused on enhancing MRI contrast agent *in vivo* lifetime, efficiency, and functionality by incorporating gadolinium into nanoscale templates. Because of their increased size in comparison to the clinically employed chelates, Gd nanoparticles provide increased in vivo circulation time and also contain higher concentrations of Gd^{3+} per contrast agent, which when targeted, yield superior MRI relaxivities.[19−28] Recently, a range of different methods of incorporating Gd into nanoparticle based templates have been presented in the literature with compositions, such as Gd fluoride,[19] Gd phosphate,[20] Gd oxide,[21,22] Gd encapsulated in a perfluorocarbon emulsion,[23−25] and Gd metal−organic framework (MOF) nanoparticles.[26−29] In most cases, these Gd

Received: January 20, 2011
Accepted: April 1, 2011
Published: April 01, 2011

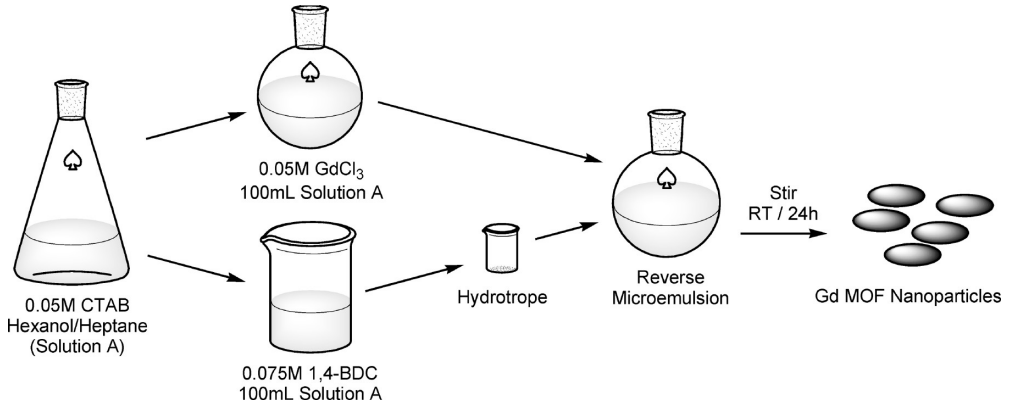

Figure 1. General route to produce Gd MOF nanoparticles via a reverse microemulsion synthesis with a hydrotrope. Cetyltrimethylammonium bromide (CTAB) is employed as a surfactant and hexanol as a cosurfactant. Gadolinium(III) chloride and 1,4-benzenedicarboxylate (1,4-BDC) form the three-dimensional nanoscale metal−organic framework.

nanoparticles have proven to be advantageous because of their increased retention times and higher relaxivities than Gd chelates. Of particular interest are the Gd MOF nanoparticles first discussed by Lin et al., these Gd MOF nanoparticles synthesized using a reverse microemulsion technique showed significantly enhanced relaxivity properties, up to an order of magnitude better than liposomal Gd chelates.[26,29] Despite these promising results, a high degree of particle size dispersity has to date limited their *in vivo* application.

Recently, it has become exceedingly important to have the ability to manipulate and control the size and size distribution of nanoparticles, which will be used in biological systems. Size is particularly important to take advantage of the enhanced permeation and retention (EPR) effect, which can also provide a means of enhanced imaging.[30−35] The EPR effect allows for a passive targeting mechanism by utilizing the "leaky" nature of a tumor's endothelium to uptake nanoparticles. Furthermore, ease of clearance of the particles from a tumor is impaired resulting in longer retention times allowing for enhanced imaging of the tumor. Though an optimal particle size to take advantage of the EPR effect is still widely debated, the general consensus seems to be particles in the size range of 50−150 nm should prove to be most effective for a passive targeting mechanism.[30−33] For rod-shaped nanoparticles, this measurement refers to the length as it is the most commonly reported nanoparticle dimension for the EPR effect. It has been noted in the literature that rod-shaped nanoparticles are specifically advantageous as they are up taken by cells preferentially in comparison to spherical particles.[36−38] To date, there has been minimal research on determining routes to effectively control both the size and size distribution of Gd MOF nanoparticles.[26,28] Additionally, to the best of our knowledge, there has been no work presented on the effect of Gd MOF nanoparticle size on their relaxivity properties.

Gd MOF nanoparticles are synthesized *via* a reverse microemulsion procedure and incorporation of molecules that may alter the micelle itself is of particular interest. For example, it has been shown that the addition of a hydrotrope, defined as a compound that exhibits both hydrophobic and hydrophilic properties, can effectively change the rigidity of an *oil-in-water* micelle.[39−48] Therefore it would be interesting to determine if by manipulating the reverse micelle, in the case of the Gd MOFs, a simple route could be developed to tune the size and size distribution of the nanoparticles formed. Our work will present

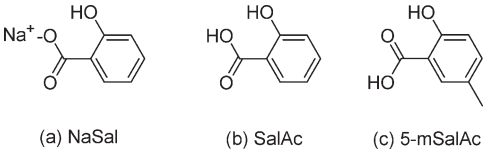

Figure 2. Hydrotropes used in the synthesis of Gd MOF nanoparticles: (a) sodium salicylate (NaSal), (b) salicylic acid (SalAc), and (c) 5-methylsalicylic acid (5-mSalAc).

the effect of the addition of a range of hydrotropes on Gd MOF nanoparticles synthesized via a reverse microemulsion method (Figure 1). Specifically, this study investigated the incorporation of hydrotropes into a Gd MOF reverse microemulsion system. The effects on nanoparticle shape, size, and size distribution were studied with respect to type and concentration of hydrotrope, along with changes in the bridging ligand used to prepare the Gd MOF nanoparticle. The three hydrotropes employed were sodium salicylate (NaSal), 5-methylsalicylic acid (5-mSalAc), and salicylic acid (SalAc) (Figure 2), because of the great deal of literature which has confirmed each of these compounds to be effective in *oil-and-water* micelle structure manipulation. Each hydrotrope proved to be an effective means of controlling both the shape and relative size of Gd MOF nanoparticles formed. The trends in the surface area, volume of nanorod, and Gd^{3+} per nanorods indicate that the surface area is the most important factor that influences the relaxivity values. This study shows that Gd MOF nanoparticles exhibit higher relaxivity values compared to the commonly administered positive contrast agent, Magnevist, and most importantly the Gd MOFs synthesized at 82 nm in length with addition of NaSal show the highest reported longitudinal relaxivity ($R1$) values.

EXPERIMENTAL SECTION

Materials. Cetyltrimethylammonium bromide (CTAB) (Sigma Ultra, 99%), gadolinium(III) chloride ($GdCl_3$) (99.999%), terephthalic acid (98%), 1,2,4-benzenetricarboxylic acid (>99%), NaSal (99.5%), hexanol (98%), methylamine solution (40 wt % in water), and xanthan gum were purchased from Sigma-Aldrich. 5-mSalAc (98%) was purchased from Acros Organics. Heptane (HPLC grade), SalAc (ACS grade, crystal), and nitric acid were purchased from Mallinckrodt Chemicals. Deionized ultrafiltered (DIUF) water and ethanol were

Table 1. Effect of NaSal as a Hydrotrope on Gd MOF Nanoparticle Dimensions

w	bridging ligand[a]	NaSal (μM)[b]	length (nm)[c]	% RSD[d]	width (nm)[c]	% RSD[d]	aspect ratio[e]
8	1,4-BDC	0	93	44	42	59	2
10	1,4-BDC	0	122	50	46	50	3
8	1,4-BDC	135	82	25	17	22	5
10	1,4-BDC	67.5	112	32	23	22	5
10	1,4-BDC	135	114	33	25	22	5
10	1,4-BDC	270	156	31	28	23	6
10	1,4-BDC	405	146	32	24	20	6
10	1,4-BDC	440	145	34	25	26	6
10	1,4-BDC	470	149	28	29	22	5
10	1,4-BDC	540	159	25	26	21	6
16	1,2,4-BTC	0	70	30	39	41	2
22	1,2,4-BTC	0	113	30	56	30	2
16	1,2,4-BTC	3050	24	34	17	26	1
22	1,2,4-BTC	3050	98	27	70	32	1

[a] 1,4-BDC and 1,2,4-BTC are defined as 1,4-benzenedicarboxylate and 1,2,4-benzenetricarboxylate methyl ammonium salts, respectively. [b] Gd MOF nanoparticles synthesized via the standard route from the literature with no incorporation of NaSal (0 μM). [c] A minimum of 500 particles were measured and averaged from at least five independent batches of Gd MOF nanoparticles. [d] % RSD is defined as percent relative standard deviation. [e] Aspect ratio is defined as the length divided by the width of the Gd MOF nanoparticle.

purchased from Fisher. Gadopentetate dimeglumine (Magnevist) was obtained from Berlex. All chemicals, unless specified, were reagent grade and used as received.

Synthesis of 1,4-Benzenedicarboxylate (1,4-BDC) and 1,2,4-Benzenetricarboxylate (1,2,4-BTC) Methyl Ammonium Salts. Either terephthalic acid (10 g) or 1,2,4-benzenetricarboxylic acid (10 g) was concentrated in a methyl amine solution (40 wt.% water). The solvent was then removed via rotary evaporation and the remaining salt was dried overnight in a vacuum oven.

Formation of Gd MOF Nanoparticles via the Standard Route from the Literature. Gd MOF nanoparticles were synthesized via a reverse microemulsion system developed by Reiter and coworkers[26] employing 0.05 M $GdCl_3$, 0.05 M CTAB, as the surfactant, and 0.075 M 1,4-BDC or 0.05 M 1,2.4-BTC, as the chelating agent. The 1,4-BDC was utilized at a water-to-surfactant ratio, *w*, of 8 or 10, while the 1,2,4-BTC was employed using either a *w* value of 16 or 22. Briefly, a stock suspension was produced of CTAB (1.3766 g, 0.05 M) in heptane (216.6 mL) and hexanol (23.5 mL). In a beaker equipped with a stir bar, CTAB suspension (100 mL) was combined with either 1,4-BDC solution (0.075 M) or 1,2,4-BTC solution (0.05 M) and allowed to stir for 15 min. In a 250 mL Pyrex bottle equipped with a stir bar, CTAB suspension (100 mL) was combined with $GdCl_3$ solution (0.05 M) and allowed to stir for 15 min. Exact volumes of 1,4-BDC, 1,2,4-BTC, and $GdCl_3$ were determined based on the targeted *w* value. The 1,4-BDC or 1,2,4-BTC solution was then added into the $GdCl_3$ solution. The combined reverse microemulsion was then allowed to stir in a sealed bottle at room temperature for 24 h. After 24 h, the microemulsion was centrifuged at 5000 rpm for a total of 30 min. After removal of the supernatant, the particles were washed with ethanol (15 mL), sonicated, and then recentrifuged for 30 min. The supernatant was discarded. The particles underwent an additional cycle of dispersement in ethanol (15 mL), sonication, and centrifugation, to remove any excess reactants. The particles then underwent a cycle of dispersement in DIUF water (15 mL), sonication, and centrifugation. Finally, the particles were redispersed in DIUF water for both transmission electron microscopy (TEM) and inductively coupled plasma-atomic emission spectroscopy (ICP-AES) characterization.

Formation of Gd MOF Nanoparticles with Addition of Hydrotrope. Gd MOF nanoparticles were synthesized via a similar route as discussed above. A stock suspension of CTAB (1.3766 g, 0.05 M) in heptane (216.6 mL) and hexanol (23.5 mL) was prepared. $GdCl_3$ (0.05 M), 1,4-BDC (0.075 M), and 1,2,4-BTC (0.05 M) solutions were prepared. In a beaker equipped with a stir bar, an aliquot of the CTAB suspension (100 mL) was combined with either 1,4-BDC solution (0.075 M) or 1,2,4-BTC (0.05 M) and allowed to stir for 15 min. In a 250 mL Pyrex bottle equipped with a stir bar, a second aliquot of the CTAB suspension (100 mL) was combined with $GdCl_3$ solution (0.05 M) and allowed to stir for 15 min. Exact volumes of 1,4-BDC, 1,2,4-BTC, and $GdCl_3$ were determined based on the targeted *w* value. The hydrotrope was then measured into a scintillation vial and transferred to the $GdCl_3$ flask via multiple rinses with the 1,4-BDC solution. The combined reverse emulsion was then allowed to stir in a sealed bottle at room temperature for 24 h. After 24 h, the microemulsion was centrifuged at 5000 rpm for a total of 30 min. After removal of the supernatant the particles were washed with ethanol (15 mL), sonicated, and then recentrifuged for 30 min. The supernatant was discarded. The particles underwent an additional cycle of dispersement in ethanol (15 mL), sonication, and centrifugation, in an attempt to remove any excess reactants. The particles then underwent a cycle of dispersement in DIUF water (15 mL), sonication, and centrifugation. Finally, the particles were redispersed in DIUF water for both TEM and ICP-AES characterization.

Characterization. TEM was performed on a Philips CM200 with an accelerating voltage of 200 kV. A Keen View Soft Imaging System coupled to iTEM Universal TEM Imaging Platform Software was utilized to acquire digital TEM images. ImageJ (National Institute of Health, Bethesda, MD), an image processing and analysis software, was employed to measure length and width properties of Gd MOF nanoparticles. Each dimension shown in Table 1 and 2 is an average of at least 500 nanoparticles from three independently synthesized batches of Gd MOF nanoparticles. Longitudinal relaxation time ($T1$)-weighted MRI was performed using a 4.7 T Bruker PharmaScan instrument. Briefly, Gd MOF nanoparticles at a range of serial dilutions were suspended in 0.02% xanthan gum/DIUF water solution in microcentrifuge tubes, as has been previously discussed in the literature.[26] Tubes were then placed onto the custom designed holder and inserted into a Bruker volume coil (62 mm diameter). The coil, tuned to the ^1H frequency of 200 MHz, was used for radiofrequency RF transmission and receiving. Rapid acquisition with relaxation enhancement (RARE) $T1$-weighted scans were performed with various echo times (TE). The following parameters

Table 2. Effect of 5-mSalAc and SalAc as Hydrotropes on Gd MOF Nanoparticles Synthesized at $w = 10$

5-mSalAc (μM)	length (nm)[a]	% RSD[b]	width (nm)[a]	% RSD[b]	aspect ratio[c]
67.5	127	39	23	25	6
135	136	41	23	21	6
270	160	38	23	25	7
405	207	36	27	25	8
440	527	44	40	28	13
470	1000	39	90	26	11
540	1000	35	81	19	12
SalAc (μM)	length (nm)[a]	% RSD[b]	width (nm)[a]	% RSD[b]	aspect ratio[c]
67.5	116	26	42	48	3
135	106	15	31	21	3
270	297	44	44	31	7
405	252	50	39	23	6
440	445	47	48	26	9
470	1170	32	90	21	13
540	1350	32	113	25	12

[a] A minimum of 500 particles were measured and averaged from at least five independent batches of Gd MOF nanoparticles. [b] %RSD is defined as percent relative standard deviation. [c] Aspect ratio is defined as the length divided by the width of the Gd MOF nanoparticle.

were used: field of view 6.0 cm, slice thickness 2.0 mm, with 2 axial or sagittal slices, matrix size 128 × 128, relaxation time = 600, 800, 1000, 1200, 1400, 1600, 1800, 2000, 2500, 3000, 3500, and 4000 ms, TE = 50.8 ms, number of averages 1, total scan time 12 min and 14 s. The calculations of $T1$ values were performed automatically for a selected region of interest using Bruker ParaVision software (Version 3.0, Bruker Medical, Billerica, MA) according to the equation $y = A + C(1 - e^{-t/T1})$. ICP-AES data was acquired on a Perkin-Elmer Optima 3000 ICP-AES instrument following the EPA 200.7 standardized method. The instrument was calibrated with an internal scandium standard and recalibrated if there was greater than 20% drift from the 50 ppm concentration. Gd MOF nanoparticle samples were diluted in a 2% nitric solution and run against an internal quality control gadolinium standard from High Purity Standards using a five point calibration.

RESULTS AND DISCUSSION

MRI is arguably one of the most powerful diagnostic imaging techniques because of its noninvasive nature and resolution. In MRI, a magnetic field aligns proton spins in the body; low-intensity radio frequency electromagnetic waves are then pulsed to disrupt the proton's alignment with the magnetic field. The protons relax to their original alignment once the radiofrequency is ceased, producing a nuclear magnetic resonance reflecting the spatial distribution of proton densities. MRI is widely used clinically for imaging of various soft tissues to identify pathological processes and is the premier technique for imaging cancer and other advanced diseases. Contrast agents are regularly employed in diagnostic MRI to attain higher resolution physiological images.[49−51] Contrast agents indirectly affect the signal by significantly altering the $T1$ or transverse relaxation times ($T2$) because of their dipole−dipole interaction with water protons. Negative contrast agents, such as iron-based nanoparticles, affect the $T2$ relaxation time but are rarely used in the clinical setting due to their limitations with respect to dynamic range, void separation, and toxicity.[49−53] Conversely, positive contrast agents, such as Magnevist, are predominantly used in the clinic. These are based on Gd chelates and greatly decrease the $T1$ relaxation time. Despite their wide clinical use, Gd chelates have several limitations including short *in vivo* retention times, limited relaxation properties, along with being difficult to modify for more advanced diagnostic capabilities.[49−53] As such, Gd based nanoparticles have gained a great deal of interest as diagnostic and nanomedicine platforms due to their potential for increasing retention times and introduction of increased functionality, such as targeting ligands and therapeutics, along with yielding enhanced imaging through both changes in their physical and chemical properties.[20,22,26,29,54−57] Although a great deal of interest has focused on modification of the surface of these nanoparticles, as of late, there is limited research on how shape and size properties of the Gd nanoparticles affect MRI relaxation rates.

Synthesis of Gd MOF Nanoparticles with Hydrotropes. Gd-based nanoparticles have shown a great deal of promise toward positive contrast agents for MRI.[20,22,26,29,54−57] In particular, Lin et al. have shown enhanced $T1$ relaxation properties with Gd MOF nanoparticles synthesized via a reverse microemulsion technique.[26,28,29] Our group has recently shown that modifying the Gd MOFs with a range of polymers can greatly affect their final MRI properties.[56,58] It has also been reported that the size of these Gd MOF nanoparticles can be varied by changing the w value, the choice of bridging ligand and cosurfactant, and the temperature of the reaction.[26,28] To date, there have been no studies to examine the effect of hydrotropes on reverse micelle systems forming nanoscale MOFs or the overall effect of their size with respect to MRI relaxation properties. The amphiphilic nature of hydrotrope molecules provides the ability to significantly increase the solubility of slightly soluble organic compounds in water. At a minimum hydrotrope concentration, hydrotropes begin to self-associate, but cannot form well organized self-assemblies such as micelles without the addition of a surfactant.[42] Experimental studies which incorporated hydrotropes into *oil-in-water* micelles, with CTAB as the surfactant, show a transition from spherical/ellipsoidal to worm-like micelles.[39,40,44−46] It is expected that the same effect may be observed for reverse microemulsion systems involving the surfactant CTAB, such as the system which forms Gd MOF nanoparticles.

Herein, we employ a combination of the literature procedure to synthesize Gd MOF nanoparticles with the addition of a range of hydrotropes in an attempt to control the shape, size, and size distribution of the nanoparticles formed. First, Gd MOF nanoparticles were synthesized via the standard route from the literature with a reverse microemulsion system of heptane, hexanol, and CTAB (0.05 M). The addition of $GdCl_3$ (0.05 M) and 1,4-BDC (0.075 M) or 1,2,4-BTC (0.05 M) solutions at a range of w values successfully produced Gd MOF nanoparticles (Figure 3a-3d). Gd MOF nanoparticles synthesized with the 1,4-BDC ligand provided an average length near 100 nm with the general composition of $Gd(1,4\text{-}BDC)_{1.5}(H_2O)_2$ (Figure 3a−b and Table 1). Nanoparticles that employed 1,2,4-BTC as a bridging moiety yielded Gd MOF nanoparticles with average lengths between 70 and 113 nm and a general composition of $Gd(1,2,4\text{-}BTC)(H_2O)_3 \cdot H_2O$ (Figure 3c−d and Table 1). All four Gd MOF nanoparticles synthesized via the standard route

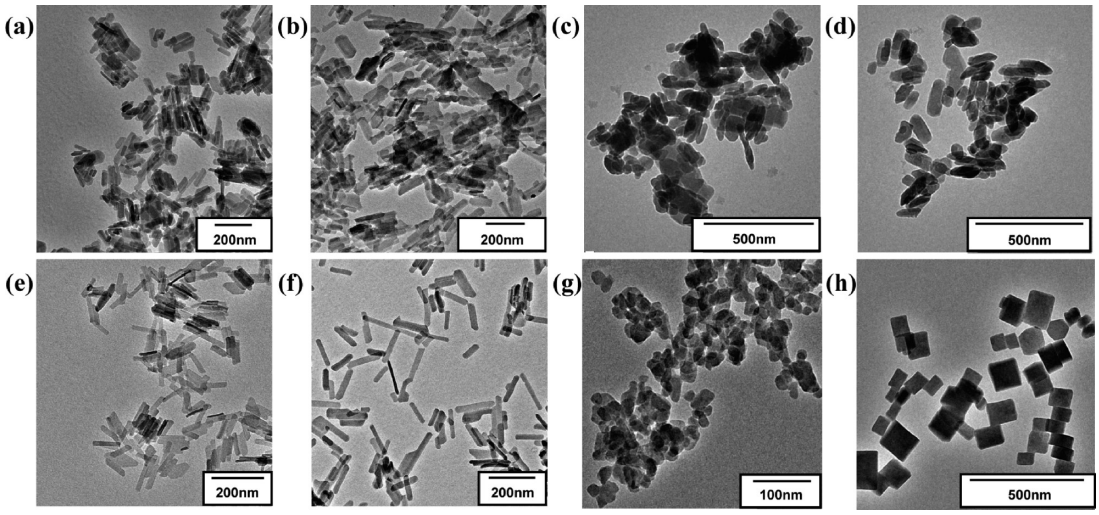

Figure 3. Transmission electron microscopy of Gd MOF nanoparticles synthesized *via* a reverse microemulsion utilizing 0.05 M CTAB, 0.05 M $GdCl_3$, and (a) 0.075 M 1,4-BDC at $w = 8$, (b) 0.075 M 1,4-BDC at $w = 10$, (c) 0.05 M 1,2,4-BTC at $w = 16$, (d) 0.05 M 1,2,4-BTC at $w = 22$, (e) 0.075 M 1,4-BDC, 135 μM NaSal at $w = 8$, (f) 0.075 M 1,4-BDC, 135 μM NaSal at $w = 10$, (g) 0.05 M 1,2,4-BTC, 3050 μM NaSal at $w = 16$, and (h) 0.05 M 1,2,4-BTC, 3050 μM NaSal at $w = 22$.

from the literature[26] yielded broad particle size distributions (Table 1), as can be seen by the high percent relative standard deviation (%RSD) values in both the nanoparticle length and width. In an effort to reduce the size distribution of the Gd MOF nanoparticles, three different hydrotropes, NaSal, 5-mSalAc, and SalAc, were integrated into the reverse microemulsion synthesis. Each of these hydrotropes have been reported to control the size and morphology of *oil-in-water* micelles,[39,40,44−46] and it is hypothesized that these hydrotropes will also enable more control over nanoparticle size and provide reduced size distributions for the Gd MOF nanoparticles synthesized by the reverse microemulsion method.

Influence of Sodium Salicylate on Gd MOF Nanoparticle Size. The addition of NaSal into *oil-in-water* micelles formed using the surfactant CTAB has been shown to cause a transition from spherical/ellipsoidal to worm-like micelles at varying concentrations.[44,46] It is hypothesized that the same trend would be expected for the addition of NaSal to reverse microemulsion systems, which potentially provides a mechanism to control particle size and reduce particle size distribution. As such, Gd MOF nanoparticles were synthesized by a reverse microemulsion as reported earlier;[26] however, NaSal was incorporated into the final microemulsion during the combination of the two reverse microemulsions of $GdCl_3$ and 1,4-BDC. Gd MOF nanoparticles at w values of 8 and 10 were synthesized with the addition of a range of concentration of NaSal to directly compare with Gd MOFs synthesized without any hydrotrope at the same w value. An increase in the concentration of NaSal at a constant w value of 10, from 67.5 μM to 540 μM, confirmed both an increase in length and decrease in diameter in comparison to those Gd MOF nanoparticles made without NaSal (Figure 3e−f and Table 1). This can be more clearly seen with comparison of the average aspect ratios (Table 1), defined as the length divided by width of the nanoparticles, with respect to NaSal concentration. As NaSal concentration increases, the aspect ratio of the Gd MOF nanoparticles triples in most cases (Table 1). This is particularly interesting from a passive targeting approach, as it has been previously discussed that nanoparticles with higher aspect ratios, or more rod-like character, should be up taken by the EPR effect preferentially to spheres.[36−38]

The Gd MOF nanoparticles synthesized with a combination of 1,2,4-BTC, as the bridging ligand, and NaSal, as the hydrotrope, showed decreases in the average length and width dimensions (Figures 3g−h and Table 1). Unfortunately, there were not large decreases in the particle length or width distributions. The Gd MOF nanoparticles with a length of 24 nm may be useful for comparison of size versus cellular uptake and $T1$ relaxation properties. Overall, the Gd MOF nanoparticles formed from a reverse microemulsion system, with the addition of NaSal as a hydrotrope, showed significant changes in their overall shape and size distributions. Furthermore, addition of NaSal when employed with the 1,4-BDC bridging ligand yielded particles with a much lower particle size distribution in comparison to Gd MOFs synthesized via the standard route from the literature.[26]

Influence of 5-Methylsalicylic Acid on Gd MOF Nanoparticle Size. Literature on incorporation of 5-mSalAc into *oil-in-water* CTAB-based micelles suggests that the addition of 5-mSalAc also promotes elongation to worm-like micelles.[39,42,59] Although 5-mSalAc has a similar structure to NaSal, Figure 2, it is hypothesized that the addition of an acid moiety and methyl group on the aromatic ring may screen the repulsive electrostatic forces between the surfactant head groups of the CTAB yielding a more worm-like micelle structure.[42] Despite these changes in hydrotrope structure, it is hypothesized that similar effects will be observed in a reverse microemulsion produced with 5-mSalAc in comparison to NaSal. When Gd MOF nanoparticles were synthesized with and without 5-mSalAc, the nanoparticles synthesized with 5-mSalAc showed a significant decrease in width, nearly half, with respect to the %RSD, Table 2. The Gd MOF nanoparticles became increasingly longer as the concentration of 5-mSalAc was increased (Table 2, Figure 4a-b, and Supporting Information S1). Increasing the 5-mSalAc concentration to 440 μM yielded a dramatic increase in the average length to 527 nm (Figure 4b, Table 2, and Supporting Information S1), while 540 μM 5-mSalAc produced Gd MOF nanoparticles with lengths in the micrometer range (Table 2 and Supporting Information S1).

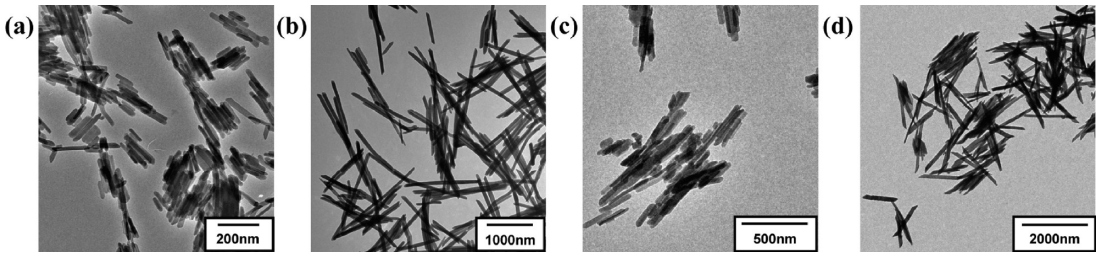

Figure 4. Transmission electron microscopy of Gd MOFs synthesized at $w = 10$ with (a) 270 μM 5-mSalAc, (b) 540 μM 5-mSalAc, (c) 270 μM SalAc, and (d) 540 μM Sal.

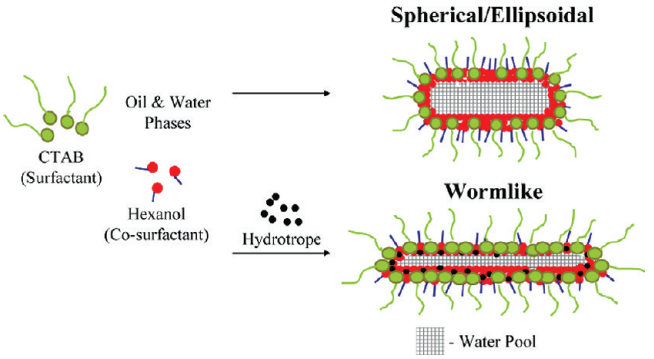

Figure 5. Schematic of a hydrotrope in a reverse microemulsion.

The diameter of the Gd MOF nanoparticles decreased with the introduction of 5-mSalAc yielding particles with significantly larger aspect ratios (Table 2). Unlike the Gd MOF nanoparticles formed with the addition of NaSal, which seemed to have a 'locked-in' width of around 25 nm, these particles showed a noticeable increase in width with increase in 5-mSalAc concentration (Table 2). Results from the 5-mSalAc studies demonstrate a significantly larger influence on the Gd MOF nanoparticle size in comparison with NaSal producing particles in the micrometer range in length.

Influence of Salicylic Acid on Gd MOF Size. Literature has taken advantage of SalAc in *oil-in-water* micelles to provide elongated structures with worm-like morphologies. Much like the addition of NaSal and 5-mSalAc into *oil-in-water* emulsions, SalAc is also expected to affect the overall dimensions of a reverse micelle. Although we have confirmed that NaSal and 5-mSalAc change the micelle significantly when added to a reverse microemulsion system, to fully understand the influence of the hydrotrope chemical structure on the reverse micelle, SalAc was also studied. As with 5-mSalAc, the addition of SalAc increased the lengths, widths, and aspect ratios of the Gd MOF nanoparticles with increasing hydrotrope concentration (Table 2 and Figure 4c–d). As the SalAc concentration increased to 270 μM SalAc, the Gd MOF nanoparticles formed were much more disperse in both their length and width dimensions with respect to %RSDs (Figure 4c and Table 2). In all cases the addition of SalAc to the reverse microemulsion system yielded particles with significantly increased aspect ratio (Table 2), suggesting these rod-like particles might be effective for passive targeting through the EPR effect.

Effect of a Hydrotropes on Reverse Microemulsion System. Reported studies indicate that with the addition of hydrotropes to *oil-in-water* CTAB-based micelles, there is an observed transition from spherical/ellipsoidal micelles into worm-like shapes.[39,40,44−46] In *oil-in-water* micelles which include a hydrotrope, literature suggests that the carboxylic head of a hydrotrope aligns next to the head of the surfactant, and the hydrophobic part of the hydrotrope orientates close to the tail of the surfactant.[42] This ordered alignment between the surfactant and hydrotrope screens the electrostatic repulsion between the CTAB head groups allowing the CTAB to pack tighter together, reducing the micelle curvature and promoting growth along the axial position, yielding a micelle with a larger aspect ratio (Figure 5).

It is expected that parameters that influence *oil-in-water* emulsions will also have similar effects in reverse microemulsion systems. As such the same interactions between a hydrotrope and the surfactant in the reverse micelle are expected to occur. In our studies with the addition of all three hydrotropes to the reverse microemulsion system, results compared quite closely to *oil-and-water* emulsions with the incorporation of a hydrotrope. In nearly all cases, the addition of NaSal, 5-mSalAc, or SalAc yielded Gd MOF nanoparticles with longer length and narrower width dimensions, suggesting an increase in the elongation of the reverse micelles formed. As such, it is hypothesized that the length and diameter of the reverse micelle changed with the addition of each of the hydrotropes due to tighter packing of the surfactant heads of the CTAB at the oil−water interface. Increased concentrations in hydrotrope provided closer packing, which reduced the electrostatic repulsion of the CTAB head groups. The reduction in electrostatic repulsion causes an axial elongation of the micelles and a transition from an ellipsoidal micelle to a more rigid worm-like structure.

The decrease in size distribution of the Gd MOF nanoparticles suggests that the incorporation of hydrotropes into a reverse microemulsion produce micelles with a much more rigid structure in the axial dimension. It is hypothesized that this increase in rigidity is an effect of an increase in the end-cap energy of the micelle and the chemical structure of the hydrotrope. The results are in agreement with reports that show when the hydrotrope concentration is increased the surfactant and hydrotrope will favor aligning in a linear manner reducing the curvature of the micelles in order to decrease the energy of the system. Furthermore, the chemical structures of the hydrotropes used are very similar (Figure 2), with either a change in counterion or substituent. It has been reported that the pH of the aqueous droplet affects the formation of reverse micelles.[48,60,61] Because NaSal, 5-mSalAc, and SalAc can, and likely do, undergo dissociation at the aqueous interfacial pool, the pH of the water droplet may be affected differently. Our data suggests that the smaller H^+ ion may promote higher packing of the surfactant at the micelle interface. Increased dissociation of the acidic group leads to lower water droplet pH and higher surface packing of the CTAB head

Table 3. Gd MOF Nanoparticle Physical Properties with Respect to MRI Relaxivity Properties

contrast agent	volume (nm^3)[b]	total surface area (nm^2)[b]	Gd^{3+} (atoms per particle)[c,d]	$R1$ ($mM^{-1}\ s^{-1}$)[e]	$R2$ ($mM^{-1}\ s^{-1}$)[e]	$R2/R1$
Magnevist				4.3	5.5	1.3
Gd MOF (24 nm)[a]	9.79×10^3	3.92×10^{19}	3.76×10^4	70.1	105.4	1.5
Gd MOF (82 nm)[a]	1.86×10^4	4.51×10^{19}	6.45×10^4	83.9	98.2	1.2
Gd MOF (112 nm)[a]	4.65×10^4	3.33×10^{19}	1.61×10^5	69.3	88.3	1.3
Gd MOF (146 nm)[a]	6.60×10^4	3.13×10^{19}	2.29×10^5	31.4	37.5	1.2
Gd MOF (207 nm)[a]	1.19×10^5	2.74×10^{19}	4.11×10^5	29.4	39.6	1.3
Gd MOF (527 nm)[a]	6.62×10^5	1.80×10^{19}	2.29×10^6	22.1	31.8	1.4
Gd MOF (1001 nm)[a]	5.16×10^6	0.893×10^{19}	1.79×10^7	17.8	24.4	1.4

[a] Values in parentheses are average lengths of Gd MOF nanoparticles (Table 1 and 2). [b] Experimental volumes and surface areas for each Gd MOF sample were determined assuming a cylindrical shape (with the exception of the Gd MOF (24 nm) which was assumed to be a cube) and utilizing length and width values determined by TEM. [c] Gd^{3+} concentrations were determined by ICP-AES. [d] Gd^{3+} (atoms per nanoparticle) values were determined as previously discussed in the literature.[28] [e] relaxivity values were determined using a 4.7 T MRI scanner in a 0.2% xanthan gum solution.

groups, which elongate the micelles. This observation can be attributed to the protons further reducing the electrostatic repulsion between the surfactant's headgroup; therefore the higher the concentration of protons, the more elongated the micelles, which was confirmed by creating longer particles (Table 1 and 2). Further work is focused on manipulating the counterion size to determine effects on micelle shape.

Furthermore, it could be hypothesized that the addition of substituents may cause steric effects in turn decreasing surfactant packing. Comparing the chemical structures of 5-mSalAc and SalAc, demonstrates only a methyl substituent difference in structure (Figure 2). In this case, Gd MOF nanoparticles synthesized with 5-mSalAc and SalAc yielded particles with nearly identical dimensions up to a concentration of 440 μM hydrotrope. Once the concentration of SalAc was increased the lengths of the Gd MOF nanoparticles showed significant increases up to 1350 nm at a concentration of 540 μM SalAc. This trend suggests that the addition of a methyl substituent to the hydrotrope decreases the ability of CTAB head groups to pack closely, while the SalAc structure provides a closer packing.

In an attempt to confirm the Gd MOF nanoparticle chemical structure is not affected by changes in size, ATR-FTIR spectroscopy was employed. Each of the ATR-FTIR spectra (Supporting Information *S2*) from Gd MOF nanoparticles synthesized at a range of differing sizes appeared to be identical. Each Gd MOF particle sample showed the characteristic out-of-plane =C−H aromatic stretch at 725 cm^{-1}, symmetric carboxylate stretch at 1400 cm^{-1}, an asymmetric carboxylate stretch at 1540 cm^{-1}, along with peaks at 2855 cm^{-1}, 2925 cm^{-1}, and 3065 cm^{-1}, which are attributed to the −C-H stretching vibrations of the 1,4-BDC bridging ligand, and 3460 cm^{-1}, which is attributed to the −OH stretch of the water ligand. Powder X-ray diffraction patterns were utilized to determine the crystalline structure of Gd MOF nanoparticles with respect to changes in size (Supporting Information *S3*). In each case, Gd MOF nanoparticles showed similar diffraction patterns to those originally synthesized without the addition of a hydrotrope by Rieter et al. and the known crystalline phase for $Tb(1,4\text{-}BDC)_{1.5}\text{-}(H_2O)_2$ reported by Reineke et al.[26,62] Powder X-ray diffraction patterns suggest an extended 3D, triclinic topology with an overall unit cell structure of $Gd_2(1,4\text{-}BDC)_3(H_2O)_4$, where each Gd atom binds to six oxygen atoms from the 1,4-BDC bridging ligands and two oxygen's from coordinated water.[26,62]

***T*1 Relaxation Properties with Respect to Gd MOF Nanoparticle Size.** Contrast agents used in MRI enhance the contrast by decreasing the relaxation time of nearby water protons effecting either the *T*1 or *T*2 value. Generally these values are discussed as either the *R*1 or the transverse relaxivity (*R*2), respectively, and are simply the inverse of the relaxation time with respect to the concentration of contrast agent. The ratio of *R*2/*R*1 indicates the type of contrast agent; where positive contrast agents show a value of less than two and are preferred over negative contrast agents due to their brightening effect in *T*1-weighted images. Recently, Gd-based nanoparticles have proven to be desirable due to their ability to increase *R*1, which produces a brighter contrast in comparison to clinically employed Gd chelates. Gd MOF nanoparticles are predominantly being investigated as an alternative to Gd chelates because they are larger in size resulting in potentially higher retention times *in vivo*, have higher concentrations of Gd^{3+} ion per targeted contrast agent producing higher relaxivity values, and their size and surface chemistry can be easily tuned.

The relaxivity values of Gd MOF nanoparticles synthesized in these experiments were obtained by employing *in vitro* MRI using a 4.7 T scanner. A range of sizes were studied in order to provide information on the effects of Gd MOF nanoparticles physical properties on their T1 relaxation characteristics. For each sample, a series of dilutions of Gd MOF nanoparticles was prepared and the concentration of Gd^{3+} was determined by ICP-AES. The relaxivity results (Table 3 and Supporting Information S2) are shown for several Gd MOF nanoparticle samples as the calculated *R*1 and *R*2 rates for the various contrast agents with respect to their Gd^{3+} concentration. In all cases, the Gd MOF nanoparticles showed increased *R*1 values with respect to the clinical positive contrast agent, Magnevist, used for comparison. Furthermore, each of their ratios of *R*2/*R*1 are less than two confirming their ability to be employed as positive contrast agents. In this study, the Gd MOF nanoparticles provided an increased *R*1 ranging from 17.8 to 70.9 $mM^{-1}\ s^{-1}$ in comparison to 4.4 $mM^{-1}\ s^{-1}$ seen for Magnevist. For example, the Gd MOF nanoparticles with an average length of 112 nm displayed a *R*1 value of 69.3 $mM^{-1}\ s^{-1}$ yielding a *R*2/*R*1 ratio of 1.3 (Table 3). In comparison, Gd MOF nanoparticles with an average length of 1001 nm, showed a measured *R*1 value of 17.8 $mM^{-1}\ s^{-1}$, with a *R*2/*R*1 ratio of 1.4 (Table 3). As can be seen in Table 3, the smaller Gd MOF nanoparticles showed marked improvements in relaxivity. Most interesting are the Gd MOFs which were synthesized at an average length of 82 nm. The obtained *R*1 value of 83.9 $mM^{-1}\ s^{-1}$ is nearly 20 times larger than that of the Magnevist, and to the best of our knowledge, is one of the highest reported relaxivity values to date for Gd MOF nanoparticles.

As can be seen by the data, a trend of increasing relaxivity is seen with decreasing average particle length (Table 3), with the exception of the Gd MOF nanoparticles with an average length dimension of 24 nm. As such, in order to determine if there is an effect on MRI capabilities with respect to particle size, volumes and total surface areas were estimated for each of the Gd MOF particles. The volume of each nanoparticle was determined assuming a cylindrical shape using the measured dimension of length and width from TEM. The exception was the 24 nm sample, which was assumed to be a cube based upon the TEM images (Figure 3h). The total surface area of each batch of Gd MOF nanoparticles was calculated by multiplying the average surface area of one particle and the total number of particles in each sample. In order to calculate the total surface area of each batch, it was assumed that 100% of the Gd^{3+} introduced into the initial synthesis was incorporated into the final Gd MOF nanoparticles. The number of Gd^{3+} atoms per Gd MOF nanoparticle was calculated as previously discussed in the literature.[28] As the data suggests, the relaxivity values seem to follow a trend of increasing values with respect to increasing total surface area of the Gd MOF nanoparticles. For example, the Gd MOF nanoparticles with an average length of 82 nm and 6.45×10^4 Gd^{3+}/nanoparticle exhibited the highest surface area of 4.51×10^{19} nm^2 and produced the highest $R1$ value of 83.9 mM^{-1} s^{-1} (Table 3). Conversely, the largest Gd MOF nanoparticle with an average length of 1000 nm and 1.79×10^7 Gd^{3+}/nanoparticle had a total surface area of 0.893×10^{19} nm^2 and showed the lowest $R1$ value of 17.8 mM^{-1} s^{-1}. This trend is hypothesized to be due to the higher total surface area providing more Gd^{3+} ions for coordination with water. An increase in surface area of the Gd MOF nanoparticles allows for an increased number of Gd^{3+} to be available at the surface allowing for increased interaction with the surrounding water protons. This provides an increase in the $R1$ values of nanoparticles with smaller dimensions, a valuable characteristic taken advantage of in a wide range of nanoscale technologies. Furthermore, it is important to note that $R1$ does not increase with increasing amounts of Gd^{3+} per nanoparticle. Table 3 confirms that with an increase in the volume of a Gd MOF nanoparticle a decrease in the relaxivity is seen, which is hypothesized to be due to a lower number of Gd^{3+} available for coordination with water at the surface of particle. Finally, the data suggests that optimization of relaxivity properties of Gd MOF nanoparticles is closely related to their total surface area, with smaller particles offering the best relaxation properties. Specifically, the Gd MOF nanoparticles synthesized with a length of 82 nm yield enhanced imaging capabilities, along with offering the potential to take advantage of passive targeting through the EPR effect due to their rod-like shape.

CONCLUSIONS

Reverse microemulsions have been shown to be a useful technique to synthesize Gd MOF nanoparticles for use as positive contrast agents in MRI. To date, it has been quite difficult to control the shape and size properties of the nanoparticles that are produced. This study showed by incorporating hydrotropes into the reverse microemulsion, control over the Gd MOF nanoparticle size and shape could be achieved. Specifically, the three hydrotropes employed, NaSal, 5-mSalAc, and SalAc, were each introduced into the reverse microemulsion to determine effects on the nanoparticle formed. The addition of both 5-mSalAc and SalAc yielded increased lengths with respective increased concentration in hydrotrope. Although, there was a definitive decrease in the %RSD values for the widths of Gd MOF nanoparticles synthesized with these two hydrotropes, the standard deviations in length were still quite significant. The addition of NaSal to the reverse microemulsion also provided Gd MOF nanoparticles with increased lengths with respect to increased hydrotrope concentration. More interestingly, Gd MOF nanoparticles synthesized with the addition of NaSal showed decreases in both %RSD of length and width, nearly 40% and more than 50%, respectively. MRI studies demonstrated that all of the Gd MOF nanoparticles exhibit higher relaxivities than that of the conventionally employed Magnevist™. A trend was seen of increasing $R1$ values for the Gd MOF nanoparticles with respect to decreasing average length values. This trend is hypothesized to be an effect of the increase in total surface area of the Gd MOF nanoparticles yielding more Gd^{3+} available at the surface of the nanoparticles. Specifically, Gd MOF nanoparticles synthesized with an average length of 82 nm provided the highest reported $R1$ values of 83.9 mM^{-1} s^{-1}. As such, we have developed both a simple method of controlling shape, size, and size distribution of Gd MOF nanoparticles, along with displaying the effects of size of Gd MOF nanoparticles on relaxation properties.

ASSOCIATED CONTENT

Supporting Information. Additional TEM, along with $R1$ and $R2$ curves. This material is available free of charge via the Internet at http://pubs.acs.org.

AUTHOR INFORMATION

Corresponding Author
*E-mail: sboyes@mines.edu.

ACKNOWLEDGMENT

The authors would like to thank James Ranville at the Colorado School of Mines and Kendra Hasebroock at University of Colorado Health Science Center for help with method development for ICP-AES and MRI, respectively. The authors would like to express our gratitude to the Colorado Office of Economic Development and International Trade for financial support of this project.

REFERENCES

(1) Schmiedl, U.; Ogan, M.; Paajanen, H.; Marotti, M.; Crooks, L. E.; Brito, A. C.; Brasch, R. C. *Radiology* **1987**, *162*, 205–210.
(2) Schumann-Giampieri, G.; Schmitt-Willich, H.; Frenzel, T.; Press, W. R.; Weinmann, H. J. *Invest. Radiol.* **1991**, *26*, 969–974.
(3) Rebizak, R.; Schaefer, M.; Dellacherie, E. *Bioconj. Chem.* **1998**, *9*, 94–99.
(4) Casali, C.; Janier, M.; Canet, E.; Obadia, J. F.; Benderbous, S.; Corot, C.; Revel, D. *Acad. Radiol.* **1998**, *5*, S214–S218.
(5) Battistini, E.; Gianolio, E.; Gref, R.; Couvreur, P.; Fuzerova, S.; Othman, M.; Aime, S.; Badet, B.; Durand, P. *Chem.—Eur. J.* **2008**, *14*, 4551–4561.
(6) Schwickert, H. C.; Roberts, T. P. L.; Muhler, A.; Stiskal, M.; Demsar, F.; Brasch, R. C. *Eur. J. Radiol.* **1995**, *20*, 144–150.
(7) Langereis, S.; de Lussanet, Q. G.; van Genderen, M. H. P.; Backes, W. H.; Meijer, E. W. *Macromolecules* **2004**, *37*, 3084–3091.
(8) Talanov, V. S.; Regino, C. A. S.; Kobayashi, H.; Bernardo, M.; Choyke, P. L.; Brechbiel, M. W. *Nano Lett.* **2006**, *6*, 1459–1463.

(9) Wiener, E. C.; Brechbiel, M. W.; Brothers, H.; Magin, R. L.; Gansow, O. A.; Tomalia, D. A.; Lauterbur, P. C. *Magn. Reson. Med* **1994**, *31*, 1–8.
(10) Kobayashi, H.; Kawamoto, S.; Star, R. A.; Waldmann, T. A.; Tagaya, Y.; Brechbiel, M. W. *Cancer Res.* **2003**, *63*, 144–150.
(11) Bourne, M. W.; Margerun, L.; Hylton, N.; Campion, B.; Lai, J. J.; Derugin, N.; Higgins, C. B. *J. Magn Reson. Imaging* **1996**, *6*, 305–310.
(12) Eliaz, R. E.; Nir, S.; Marty, C.; Szoka, F. C., Jr. *Cancer Res.* **2004**, *64*, 711–718.
(13) van Broekhoven, C. L.; Parish, C. R.; Demangel, C.; Britton, W. J.; Altin, J. G. *Cancer Res.* **2004**, *64*, 4357–4365.
(14) Gabizon, A.; Horowitz, A. T.; Goren, D.; Tzemach, D.; Shmeeda, H.; Zalipsky, S. *Clin. Cancer Res.* **2003**, *9*, 6551–6559.
(15) Kamaly, N.; Kalber, T.; Thanou, M.; Bell, J. D.; Miller, A. *Bioconj. Chem.* **2009**, *20*, 648–655.
(16) Aime, S.; Castelli, D. D.; Crich, S. G.; Gianolio, E.; Terreno, E. *Acc. Chem. Res.* **2009**, *42*, 822–831.
(17) Ladd, D. L.; Hollister, R.; Peng, X.; Wei, D.; Wu, G.; Delecki, D.; Snow, R. A.; Toner, J. L.; Kellar, K.; Eck, J.; Desai, V. C.; Raymond, G.; Kinter, L. B.; Desser, T. S.; Rubin, D. L. *Bioconj. Chem.* **1999**, *10*, 361–370.
(18) Wen, X.; Jackson, E. F.; Price, R. E.; Kim, E.; Wu, Q.; Wallace, S.; Charnsangavej, C.; Gelovani, J. G.; Li, C. *Bioconj. Chem.* **2004**, *15*, 408–1415.
(19) Evanics, F.; Diamente, P. R.; van Veggel, F. C. J. M.; Stanisz, G. J.; Prosser, R. S. *Chem. Mater.* **2006**, *18*, 2499–2505.
(20) Hifumi, H.; Yamaoka, S.; Tanimoto, A.; Citterio, D.; Suzuki, K. *J. Am. Chem. Soc.* **2006**, *128*, 15090–15091.
(21) Louis, C.; Bazzi, R.; Marquette, C. A.; Bridot, J.-L.; Roux, S.; Ledoux, G.; Mercier, B.; Blum, L.; Perriat, P.; Tillement, O. *Chem. Mater.* **2005**, *17*, 1673–1682.
(22) Bridot, J.-L.; Faure, A.-C.; Laurent, S.; Riviere, C.; Billotey, C.; Hiba, B.; Janier, M.; Josserand, V.; Coll, J.-L.; Elst, L. V.; Muller, R.; Roux, S.; Perriat, P.; Tillement, O. *J. Am. Chem. Soc.* **2007**, *129*, 5076–5084.
(23) Yu, X.; Song, X.-K.; Chen, J.; Scott, M. J.; Fuhrhop, R. J.; Hall, C. S.; Gaffney, P. J.; Wickline, S. A.; Lanza, G. M. *Magn. Reson. Med* **2000**, *44*, 867–872.
(24) Morawski, A. M.; Winter, P. M.; Crowder, K. C.; Caruthers, S. D.; Fuhrhop, R. W.; Scott, M. J.; Robertson, J. D.; Abendschein, D. R.; Lanza, G. M.; Wickline, S. A. *Magn. Reson. Med* **2004**, *51*, 480–486.
(25) Kaneda, M. M.; Caruthers, S.; Lanza, G. M.; Wickline, S. A. *Ann. Biomed. Eng.* **2009**, *37*, 1922–1933.
(26) Rieter, W. J.; Taylor, K. M. L.; An, H.; Lin, W.; Lin, W. *J. Am. Chem. Soc.* **2006**, *128*, 9024–9025.
(27) Rieter, W. J.; Taylor, K. M. L.; Lin, W. *J. Am. Chem. Soc.* **2007**, *129*, 9852–9853.
(28) Taylor, K. M. L.; Jin, A.; Lin, W. *Angew. Chem., Int. Ed.* **2008**, *47*, 7722–7725.
(29) Rocca, J. D.; Lin, W. *Eur. J. Inorg. Chem.* **2010**, 3725–3734.
(30) Fukumori, Y.; Ichikawa, H. *Adv. Powder Technol.* **2006**, *17*, 1–28.
(31) Xing, G.; Yuan, H.; He, R.; Gao, X.; Jing, L.; Zhao, F.; Chai, Z.; Zhao, Y. *J. Phys. Chem. B* **2008**, *112*, 6288–6291.
(32) Tokumitsu, H.; Hiratsuka, J.; Sakurai, Y.; Kobayashi, T.; Ichikawa, H.; Fukumori, Y. *Cancer Lett.* **2000**, *150*, 177–182.
(33) Cho, K.; Wang, X.; Nie, S.; Chen, Z.; Shin, D. M. *Clin. Cancer Res.* **2008**, *14*, 1310–1316.
(34) Riehemann, K.; Schneider, S. W.; Luger, T. A.; Godin, B.; Ferrari, M.; Fuchs, H. *Angew. Chem., Int. Ed.* **2009**, *48*, 872–897.
(35) Xie, J.; Lee, S.; Chen, X. *Adv. Drug Delivery Rev.* **2010**, *62*, 1064–1079.
(36) Decuzzi, P.; Pasqualini, R.; Arap, W.; Ferrari, M. *Pharm. Res.* **2009**, *26*, 235–243.
(37) Decuzzi, P.; Godin, B.; Tanaka, T.; Lee, S.-Y.; Chiappini, C.; Liu, X.; Ferrari, M. *J. Controlled Release* **2010**, *141*, 320–327.
(38) Gentile, F.; Chiappini, C.; Fine, D.; Bhavane, R. C.; Peluccio, M. S.; Ming-Cheng Cheng, M.; Liu, X.; Ferrari, M.; Decuzzi, P. *J. Biomech.* **2008**, *41*, 2312–2318.
(39) Lin, Z.; Cai, J. J.; Scriven, L. E.; Davis, H. T. *J. Phys. Chem B* **1994**, *98*, 5984–5993.
(40) Hoffman, H.; Ebert, G. *Angew. Chem., Int. Ed. Engl.* **1988**, *27*, 902–912.
(41) Schubert, B. A.; Kaler, E. W.; Wagner, N. J. *Langmuir* **2003**, *19*, 4079–4089.
(42) Hodgdon, T. K.; Kaler, E. W. *Curr. Opin. Coll. Interfaces* **2007**, *12*, 121–128.
(43) Davies, T. S.; Ketner, A. M.; Raghavan, S. R. *J. Am. Chem. Soc.* **2006**, *128*, 6669–6675.
(44) Rodrigues, R. K.; da Silva, M. A.; Sabadini, E. *Langmuir* **2008**, *24*, 13875–13879.
(45) Mohanty, S.; Davis, H. T.; McCormick, A. V. *Langmuir* **2001**, *17*, 7160–7171.
(46) Shukla, A.; Rehage, H. *Langmuir* **2008**, *24*, 8507–8513.
(47) Bhat, M.; Gaikar, V. G. *Langmuir* **2000**, *16*, 1580–1592.
(48) Shikata, T.; Hirata, H. *J. Am. Chem. Soc.* **1989**, *5*, 398–405.
(49) Reichert, D. E.; Hancock, R. D.; Welch, M. J. *Inorg. Chem.* **1996**, *35*, 7013–7020.
(50) Strijkers, G. J.; Mulder, W. J. M.; van Tilborg, G. A. F.; Nicolay, K. *Anti-Cancer Agents Med. Chem.* **2007**, *7*, 291–305.
(51) Caravan, P.; Ellison, J. J.; McMurry, T. J.; Lauffer, R. B. *Chem. Rev* **1999**, *99*, 2293–2352.
(52) Sun, C.; Lee, J. S. H.; Zhang, M. *Adv. Drug Delivery Rev.* **2008**, *60*, 1252–1265.
(53) Artemov, D.; Bhujwalla, Z. M.; Bulte, J. W. M. *Curr. Pharm. Biotechnol.* **2004**, *5*, 485–494.
(54) Reynolds, C. H.; Annan, N.; Beshah, K.; Huber, J. H.; Shaber, S. H.; Lenkinski, R. E.; Wortman, J. A. *J. Am. Chem. Soc.* **2000**, *122*, 8940–8945.
(55) Oyewumi, M. O.; Mumper, R. J. *Drug Dev. Ind. Pharm.* **2002**, *28*, 317–328.
(56) Rowe, M. D.; Thamm, D.; Kraft, S.; Boyes, S. G. *Biomacromolecules* **2009**, *10*, 983–993.
(57) Csajbok, E.; Banyai, I.; Vander Elst, L.; Muller, R. N.; Zhou, W.; Peters, J. A. *Chemistry* **2005**, *11*, 4799–4807.
(58) Rowe, M. D.; Chang, C.-C.; Thamm, D.; Kraft, S.; Harmon, J. F., Jr.; Vogt, A. P.; Sumerlin, B. S.; Boyes, S. G. *Langmuir* **2009**, *25*, 9487–9499.
(59) Li, F.; Li, G. Z.; Wang, H.-Q.; Xue, Q. J. *Colloids Surf.* **1997**, *127*, 89–96.
(60) Shikata, T.; Hirata, H.; Kotaka, T. *Langmuir* **1988**, *4*, 354–359.
(61) Shikata, T.; Hirata, H.; Kotaka, T. *J. Phys. Chem.* **1990**, *94*, 3702–3706.
(62) Reineke, T. M.; Eddaudi, M.; Fehr, M.; Kelley, D.; Yaghi, O. M. *J. Am. Chem. Soc.* **1999**, *121*, 1651–1657.